Remote Sensing of Environment 114 (2010) 414–425

Contents lists available at ScienceDirect

Remote Sensing of Environment

journal homepage: www.elsevier.com/locate/rse

The infrared spectral signature of volcanic ash determined from high-spectral resolution satellite measurements

G. Gangale [a], A.J. Prata [b,*], L. Clarisse [c]

[a] Dipartimento di Ingegneria dei Materiali e dell'Ambiente, Università di Modena e Reggio Emilia, Italy
[b] Climate and Atmosphere Department, Norwegian Institute for Air Research, PO Box 100, 2027 Kjeller, Norway
[c] Spectroscopie de l'Atmosphère, Service de Chimie Quantique Photophysique, Université Libre de Bruxelles, Brussels, Belgium

ARTICLE INFO

Article history:
Received 22 June 2009
Received in revised form 21 September 2009
Accepted 23 September 2009

Keywords:
Volcanic ash
Radiative transfer
Infrared remote sensing

ABSTRACT

High-spectral resolution infrared spectra of the earth's atmosphere and surface are routinely available from satellite sensors, such as the Atmospheric Infrared Sounder (AIRS) and the Infrared Atmospheric Sounding Interferometer (IASI). We exploit the spectral content of AIRS data to demonstrate that airborne volcanic ash has a unique signature in the infrared (8–12 μm) that can be used to infer particle size, infrared opacity and composition. The spectral signature is interpreted with the aid of a radiative transfer model utilizing the optical properties of andesite, rhyolite and quartz. Based on the infrared spectral signature, a new volcanic ash detection algorithm is proposed that can discriminate volcanic ash from other airborne substances and we show that the algorithm depends on particle size, optical depth and composition. The new algorithm has an improved sensitivity to optically thin ash clouds, and hence can detect them for longer (~4 days) and at greater distances from the source(~5000 km).

1. Introduction

Identifying and observing the movement of volcanic ash clouds from space are done at Volcanic Ash Advisory Centres (VAACs) around the world in order to provide hazard warnings to general aviation. Volcanic eruptions can eject ash (composed mainly of SiO_2) into the atmosphere to great heights (more than 20 km) and hence ash can intersect air-routes. Volcanic ash is a known aviation hazard (Casadevall et al., 1996), causing multiple engine failure as well as interfering with important avionics equipment.

The identification of volcanic ash in meteorological satellite imagery is not straightforward because at visible wavelengths, depending on solar and satellite-sensor viewing geometry, ash clouds may appear similar to water and ice clouds. In single-band thermal imagery, ash clouds are identified by using high temporal frequency data which can often reveal the origin and movement of a volcanic plume or cloud, once an eruption has started or is in process. Previous publications in *Remote Sensing of Environment* by Simpson et al. (2000, 2001), Prata et al. (2001) and Tupper et al. (2004) have high-lighted and discussed some of the problems and challenges in detecting volcanic ash using two-channel infrared data. More sophisticated satellite-based detection algorithms have been devised by utilizing multiple channels in the thermal infrared, mid-infrared and visible wavelengths (e.g. Prata, 1989; Hillger & Clark, 2002a,b; Ellrod et al., 2003; Pergola et al., 2004; Pavolonis et al., 2006).

The purpose of this study is to demonstrate that measurements from high-spectral resolution infrared imagers and sounders may be exploited to provide good discrimination of ash clouds from other clouds and hence may help to overcome some of the problems discussed in the earlier papers using two-channel IR measurements. We show that the new algorithm has an increased sensitivity over a current two-channel method used with several lower spectral resolution multi-spectral scanners. We use data from the Atmospheric Infrared Sounder (AIRS) that provides imagery covering the infrared window region from 700 to 1400 cm^{-1} (7–14 μm) at approximately 0.5 cm^{-1} spectral resolution.

The paper is organised as follows: we first provide a short description of the AIRS instrument, the data analysis and processing. Then we present the AIRS observations and introduce some ideas regarding the spectral shape and principal character of the spectra of ash clouds. We use the recent Chaitén eruption in Chile (42.833°S, 72.646°W, 1120 m asl) to illustrate a new detection algorithm and we compare this to the 'reverse' absorption algorithm (Prata, 1989). A radiative transfer model is used to assess the effects of particle size, optical depth and ash composition on the spectra and we conclude with a discussion of the new algorithm and suggest areas needing further work.

2. Data analyses—AIRS

AIRS is an echelle spectrometer with channels operating over the infrared region from about 3.6 μm to 15 μm (600–2800 cm^{-1}) (Chahine et al., 2006). The spectrometer can image the earth and atmosphere below by cross-track scanning and by using the forward motion of the

* Corresponding author.
E-mail address: fpr@nilu.no (A.J. Prata).

0034-4257/$ – see front matter © 2009 Elsevier Inc. All rights reserved.
doi:10.1016/j.rse.2009.09.007

Aqua satellite platform on which it resides. For ease of analysis, the AIRS images are provided as data granules consisting of 2378 channels × 90 pixels × 135 lines. This results in a granule covering a region of approximately 1800 km wide by 2700 km long, with an instantaneous field of view (IFOV) of approximately 13.5 × 13.5 km^2 at nadir. In our analyses we have used v5.0 Level 1b data which consists of calibrated and geolocated radiances.

3. The 'reverse' absorption algorithm

The detection of volcanic ash in the atmosphere using satellite data is hampered by the presence of other absorbers including water vapour, liquid water and ice particles. Prata (1989) suggested that two channels in the infrared window between 8 and 12 μm could be used to discriminate ash clouds from water/ice clouds because the wavelength dependence of the absorption by ash, principally composed of SiO_2, is opposite or the reverse of that by water and ice. Using two-band infrared satellite imagery and a radiative transfer model it was shown that under many circumstances ash clouds could be clearly discriminated from water and ice clouds. Improvements to this algorithm to account for water vapour absorption have been suggested by Yu et al. (2002) and extensions of the radiative transfer model to calculate particle size, mass and infrared optical depth have been proposed by Wen and Rose (1994) and Prata and Grant (2001). The simplicity of the algorithm, the availability of multiband thermal satellite imagery (e.g. AVHRR, MODIS, SEVIRI and others) and the fact that the algorithm may be used during the night have seen the 'reverse' absorption algorithm receive widespread acceptance and use at Volcanic Ash Advisory Centres (VAACs) to locate hazardous ash clouds for aviation warnings, despite certain limitations (Simpson et al., 2000; Prata et al., 2001; Simpson et al., 2001).

More recently, high-spectral resolution satellite infrared measurements have become available from NASA's AIRS instrument and from EUMETSAT's IASI instrument. These instruments provide 100's of channels across the infrared window (8–12 μm) compared to the multiband imagers (e.g. AVHRR, MODIS, SEVIRI, GOES and GMS-VISSR) that typically provide 2–5 channels. With such a wealth of information now available from the high-spectral resolution sensors, it seems likely that improvements can be made over the multiband methods for detecting, discriminating and quantifying volcanic ash in the atmosphere. In the following we discuss an approach using spectral signatures that exploits the measurements' high-spectral content.

4. Spectral signatures

The AIRS spectra contain a large amount of information about the vertical temperature and moisture structure of the atmosphere and are affected by gases, aerosols, clouds and the radiative properties of earth's surface. Away from the large absorption regions due to gases (e.g. the ozone band near 1040 cm^{-1}), and within the atmospheric window region between 700 and 1400 cm^{-1}, the spectra are strongly influenced by clouds and aerosols. To illustrate the information content of the AIRS spectra, Fig. 1A shows a slice taken along a constant pixel number (approximately in a N–S orientation) of one AIRS granule (granule 187 on 3 May, 2008, 18:41–18:47UT) over the spectral region from 800 to 1130 cm^{-1}. The spectra are shown as brightness temperature differences ($BTD = BT[\nu] - BT[\nu_{ref}]$), using a reference wavenumber (ν_{ref}) of 1000 cm^{-1} (an arbitrary choice, but see later). The BTDs are generally positive, except in regions of very strong gaseous absorption (cf. the 9.6 μm O_3 band). In this example the transect passes over a cloud of ash particles erupted from Chaitén volcano in southern Chile, which began erupting at 08:00UT on 2 May, 2008. A striking feature of the spectrum is the enhanced positive BTDs near line 115, stretching from 800 to 980 cm^{-1}. This feature coincides exactly with the position of the Chaitén ash cloud (see Fig. 1B). Below this feature (lower line numbers) there is a region of strongly negative BTDs—these are associated with meteorological clouds.

The shape of the spectra in the region between 800 and 1130 cm^{-1} is sensitive to the composition, size and optical depth of clouds and aerosols and hence can be exploited to retrieve this information. We illustrate these effects by considering actual AIRS spectral measurements for six atmospheric conditions: (1) a high-level ice cloud, (2) a water cloud, (3) a clear scene, (4) desert dust, (5) a basaltic ash cloud (Etna ash), and (6) a rhyolitic ash cloud (Chaitén ash). The spectra consist of Top Of the Atmosphere (TOA) radiances as a function of wavenumber, but to illustrate the spectral signatures, the brightness temperature spectra are computed and they are normalized by dividing by the brightness temperature at a reference wavenumber and then plotted as non-dimensional spectra. Fig. 2 shows the ratio between the spectral brightness temperature (BT) and a reference brightness temperature at 1000 cm^{-1} (BT_{ref}) for the six conditions. The idea behind dividing by a reference brightness temperature is to approximate the emissivity variation of the spectra; the choice of 1000 cm^{-1} is arbitrary, but it is necessary to avoid absorption regions and the region around 1000 cm^{-1} is quite transparent. Within the region between 850 and 1000 cm^{-1}, the ratio for ice (blue line) increases with wavenumber, whereas for ash and desert dust it decreases. For a clear atmosphere there is a slight increase with wavenumber due to water vapour absorption. Water clouds generally have a slope between that of the ice cloud and the clear scene. Ice and water clouds behave this way because the radiance spectra for ice and water over this region decrease with increasing wavenumber (Smith et al., 1993), which is a consequence of the decrease in cloud emissivity with increasing wavenumber, which in turn is related to the spectral variation of the refractive indices of ice and water. This change of slope of the spectral ratio with wavenumber can be used to discriminate ash from ice, water clouds and clear scenes. For spectra of clear scenes over bare soil and desert, there is a balance between the competing effects of water vapour, which tends to increase the ratio with increasing wavenumber, and surface emissivity, which tends to decrease the ratio with increasing wavenumber. The slopes are also sensitive to the optical depth of the cloud in the scene as well as the microphysics of the cloud particles (refractive index, size, size distribution, and shape).

Ash clouds and desert dust have positive slopes in the region between 1070 and 1130 cm^{-1}, opposite to that for ice clouds and opposite to the slope in the 850–1000 cm^{-1} region. DeSouza-Machado et al. (2006) have previously exploited the spectral signature of desert dust in AIRS data to show how dust affects the optical depth at 900 cm^{-1}. They describe the dust signature as having a "V" shape depression in the 800–1200 cm^{-1} region, similar to that for our dust example. It is apparent that the spectral shapes do not vary in a linear manner with wavenumber, and as can be seen for the Chaitén ash, there is a peak in the curve at around 850 cm^{-1}. The spectral variation of ash is a consequence of the variation of the refractive index with wavenumber and this is explored in Section 6 by using a radiative transfer model and a microphysical model for ash. After analyzing many (>100 AIRS granules) spectral curves for ash clouds, it was found that a quadratic function would fit the spectral variation between 800 and 900 cm^{-1}, and linear fits were adequate between 910–980 cm^{-1} and 1070–1130 cm^{-1}. Because of the peculiar concave shape of the curves for ash clouds in the interval 800–1000 cm^{-1}, we use this as a discriminant for ash clouds and call this the "concavity algorithm".

To check on the efficacy of this approach we analyzed three months of AIRS data (approximately 900 granules) over the Australian continent, where it is unlikely that significant amounts of volcanic ash occur, to determine the frequency of occurrence of particular spectral signatures. In addition, we used the concavity algorithm on two months of global IASI data. These analyses showed that persistent negative concavity occurred only over desert regions, particularly the Sahara, and that very few "false detections" happened.

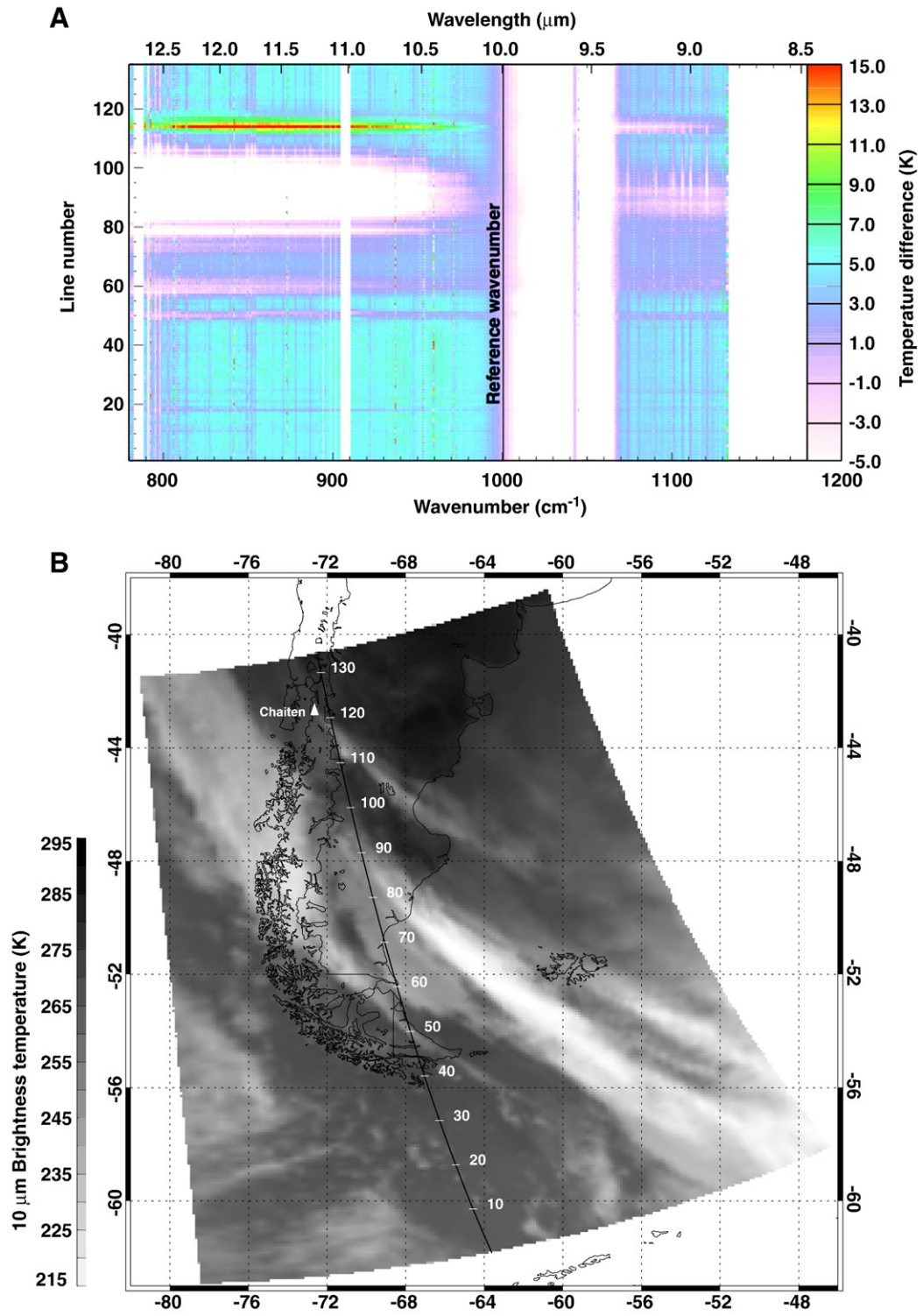

Fig. 1. (A) AIRS spectrum shown as a transect along a constant pixel number (see Fig. 1B for the location of the transect). The brightness temperature at 1000 cm^{-1} has been subtracted from the spectra and the spectra are plotted as brightness temperature differences (BTDs). Data from AIRS granule 187 on 2008/05/03. (B) 10 μm brightness temperature (K) image of one AIRS granule containing the Chaitén ash cloud and several meteorological clouds. The line shown on the image is a transect taken along a line of constant pixel number that cuts through the ash cloud and meteorological clouds. Data from AIRS granule 187 on 3 May, 2008, 18:41–1847UT.

The results of these analyses will be presented in a future paper discussing the global applicability of the concavity algorithm.

5. The concavity algorithm

The new algorithm for ash detection is based on the different behaviour of the spectral curves in the wavenumber range between 800 and 1130 cm^{-1}. The shape of these curves depends on both particle size and composition of the observed aerosol and therefore has a physical basis. The main features of these signatures (see Fig. 2) are summarized below:

1. A marked negative concavity of the Chaitén ash curve between 800 and 960 cm^{-1}.

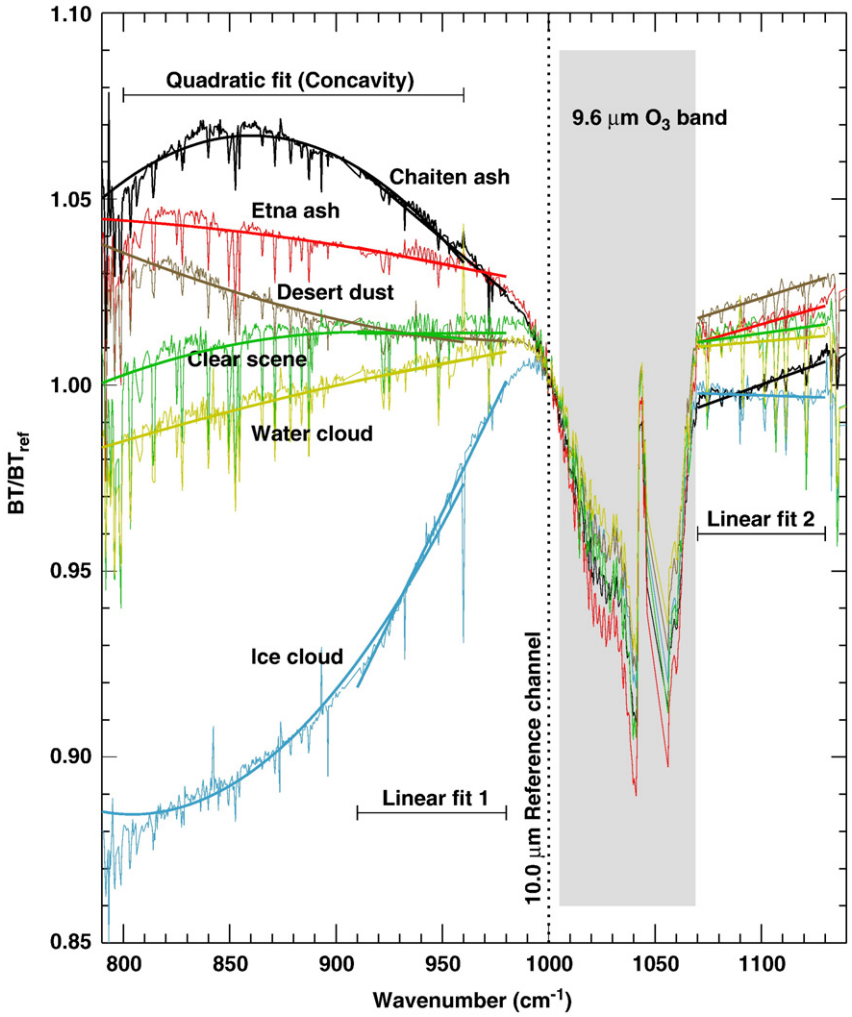

Fig. 2. Spectral ratio of the TOA brightness temperature for a single AIRS pixel and for six different scenes: (1) a pixel containing semi-transparent ice cloud (blue line: AIRS granule 187 on 2008/05/03), (2) a water cloud (yellow line: AIRS granule 101 on 2009/02/05), (3) a clear pixel (green line: AIRS granule: 101 on 2009/02/05), (4) desert dust (brown line: AIRS granule 077 2003/04/18), (5) a pixel affected by ash from an eruption of Etna (red line: AIRS granule 010 on 2002/10/30), and (6) a Chaitén ash-affected pixel (black line: AIRS granule 049 on 2008/05/05). The greyed-out region includes the strong O_3 absorption and is not used in the analyses. The spectral regions where linear and quadratic fits are performed are also indicated on the plot.

2. The curve has a maximum between 800 and 900 cm^{-1}.
3. There are different slopes of the curves between 910 and 980 cm^{-1}. In particular the signature for the ice cloud has a strong positive slope in this range while for the others it is negative or flat.
4. Different slopes of the curves between 1070 and 1130 cm^{-1}. In particular the ice cloud signature is flat or slightly negative, while the others have positive slopes.

For each pixel of the image, the curves are approximated by a polynomial function in three different intervals. A quadratic function is used to fit the curves between 800 and 960 cm^{-1} and the second degree coefficient is the concavity ($\mathcal{C}$).[1] The linear Pearson correlation coefficient ($\mathbf{r}$) is calculated in order to have a measure of the goodness of fit. Once the coefficients of the fitting parabola have been calculated, the abscissa of the maximum (ν_{max}) is also computed. Linear fits are used in the 910–980 cm^{-1} and 1070–1130 cm^{-1} intervals and the first degree coefficients are the slopes ($\mathbf{s}_1$ and $\mathbf{s}_2$, both multiplied by a factor 10^4 for convenience). Some wavenumbers have been excluded from the curve fitting because they are affected by water vapour absorption and these could be a source of error in the fit. There are many ways to exploit these estimated parameters in order to discriminate volcanic ash from other types of airborne particles and hydrometeors. Here we outline one such scheme that has worked well for some of the ash clouds we have examined; however, we caution that this scheme may not be optimum and a more detailed study using many more case studies and using both AIRS and IASI spectra is planned.

A pixel is assumed to be part of the volcanic plume if all the following conditions are satisfied:

$$\mathcal{C} < 0.0, \mathbf{r} > 0.6, \mathbf{s}_1 < 0.0, \mathbf{s}_2 > 0.0 \text{ and } 780\,cm^{-1} < \nu_{max} < 880\,cm^{-1} \quad (1)$$

It is likely that some tuning of the conditions (Eq. (1)) may be required for different ash clouds and possibly different atmospheric conditions. In particular a more robust condition, leading to fewer detections (some possibly false) has been used with $\mathcal{C} < -1.0$. This algorithm has been tested on many AIRS images of ash clouds, but we focus here on those from the Chaitén volcanic eruption, which started on 2 May 2008 (see Carn et al., 2009, for a description of the eruption). Results are compared with the 'reverse' absorption (RA) method, which is done by calculating temperature differences over narrow bands centred near to 830 cm^{-1} and 910 cm^{-1}. Integrating the AIRS radiances over the MODIS filter response functions corresponding to

[1] For convenience $\mathcal{C}$ has been multiplied by a factor 10^6.

MODIS bands 31 and 32, provides corresponding AIRS narrow band channels.

When the ash cloud becomes opaque the concavity $\mathcal{C}$ tends to zero or can even become positive, while the slope $\mathbf{s}_2$ remains positive. For this reason another set of conditions was developed to assign a pixel that contains volcanic ash,

$$\mathcal{C} > 0.0, \mathbf{r} > 0.6, \mathbf{s}_2 > 1. \tag{2}$$

The concavity algorithm produces less noisy images than the RA images, and seems to be quite sensitive to optically thin volcanic clouds. The ash plume detection is similar both over land and over the sea with no discontinuities while the RA method is affected by the thermal contrast between the ash cloud and the surface below, especially when the infrared opacity is small.

Fig. 3(A) shows $\mathcal{C}$ for two consecutive AIRS granules acquired on 3 May 2008 between 18:41 and 18:53UT. Also depicted on this figure are forward trajectories calculated from the HYSPLIT dispersion model (Draxler & Rolph, 2003). $\mathcal{C}$ varies between −0.5 and −2.5, and in this case identifies four distinct plume trajectories: two low-level plumes between 4500 m and 5200 m moving in a south-eastwards direction and two upper-level (>12,000 m) plumes travelling northwards and north-eastwards. These latter plumes were not detectable by the RA method, but are noticeable in MODIS visible wavelength imagery at the same time.

The concavity algorithm is compared to the RA method in Fig. 3(B) for another AIRS granule and an Aqua/MODIS image obtained at the same time. The two maps compare quite well; the concavity map shows no discontinuities near the coast, where the underlying surface temperature changes abruptly (from cold over the land to warmer over the sea). There is also much less noise over the land compared to the RA method which identifies large parts of the cold land surface as potentially ash-affected.[2] The greater ability of the concavity algorithm to identify ash over the land/ocean boundary and further out to sea, is probably due its greater sensitivity to optically thin clouds, since it is likely that the further the cloud is from its generating source, the thinner it will be. Spectral fits (linear) are also performed over the spectral regions, 910–980 cm^{-1} and 1070–1130 cm. The slopes of these fits are also good discriminators for ash. The ability to discriminate ash using linear fits and $\mathcal{C}$ is illustrated in the panels of Fig. 4, using AIRS data for an ash cloud from Chaitén on 5 May 2008. Each panel shows the same AIRS granule with (A) $\mathcal{C}$, (B) the slope of the linear fit across 910–980 cm^{-1}, (C) the slope of the linear fit across 1070–1130 cm, and finally (D) a brightness temperature image at around 1000 cm^{-1}. In this case the linear fits and $\mathcal{C}$ all discriminate ash well, while from single band imagery it is very difficult to discriminate ash from water/ice clouds. The RA algorithm (not shown) also discriminates ash well in this case.

For the 800–980 cm^{-1} spectral region the ability to discriminate ash follows directly from the RA algorithm, where because only two channels are available the discriminant is based on the condition:

$$T_{909} - T_{833} < 0, \tag{3}$$

where the subscripts refer to wavenumbers (cm^{-1}) at the band centres. Thus, the use of the slope as a discriminant for ash may be considered an extension of the RA algorithm and the use of the concavity a further extension, which we suggest also discriminates ash composition. This is explored further in the next section.

[2] It is possible that the land is ash-coated, as the eruption had been in progress for some time and a layer of fine ash built up over the land to the east of the volcano.

6. Optical properties and radiative transfer

Li et al. (2005) have previously demonstrated that radiative transfer modelling can be usefully applied to AIRS spectra to retrieve microphysical properties of meteorological clouds (ice and water) and they comment specifically on the use of the spectral intervals between 790–950 and 1050–1130 cm^{-1}. The spectral signatures observed in the AIRS spectra of volcanic ash clouds are similarly modelled using a radiative transfer algorithm.

The model assumes that the scattering layer is composed entirely of one substance (e.g. ash), is plane-parallel and is sufficiently high in the atmosphere that all radiative processes above the layer can be ignored. The simulation proceeds in two stages: first, the spectral radiance impinging on the lower boundary of the layer is assumed to consist of radiation emitted by the surface below and radiation that is absorbed and emitted by the atmosphere between the surface and the lower boundary of the scattering layer. This model has been used previously by Prata (1989), Wen and Rose (1994) and Prata and Grant (2001). The radiation reaching the lower boundary of the scattering layer may be written:

$$I_\nu = I_{\nu,s} t_{\nu,s} + \int_{p_s}^{p} B_\nu[T(p)] \frac{\partial t_\nu(\rho_1, \rho_2, \ldots \rho_n)}{\partial p} dp, \tag{4}$$

where, $I_{\nu,s}$ is the surface leaving radiance at wavenumber ν, p is pressure, P_s is surface pressure, t_ν is the transmittance, which is a function of absorber concentrations ρ_i, $i=1\ldots, n$, B is the Planck function and $T(p)$ is the vertical temperature profile. Eq. (4) is solved at each of the AIRS wavenumbers given the profile of temperature, and water vapour provided by a radiosonde profile and climatologies in the case of gases that are not measured by the radiosonde. The spectral radiances are computed at all AIRS wavenumbers using the Modtran-4 code (Berk et al., 1999). The lower boundary radiance is then used as input to the radiative transfer governing the scattering layer,

$$\mu \frac{\partial I}{\partial \tau}(\tau, \mu) = I(\tau, \mu) - (1 - \varpi_o) B(T) - \frac{\varpi_o}{2} \int_{-1}^{1} P(\mu; \mu') I(\tau, \mu') d\mu' \tag{5}$$

where $\tau = -\ln(-t)$ is the optical depth, μ is the cosine of the zenith angle, ϖ_o is the single scattering albedo and P is the axially-symmetric phase function. The cloud layer has an optical depth τ_1 and we are only concerned with the upwelling radiance in the direction μ at the cloud top ($t=0$). We have omitted the notation for wavenumber dependence for convenience. The boundary conditions are no downward radiance incident on the cloud top,

$$I(0, -\mu) = 0, \tag{6}$$

and the upward radiance incident on the cloud base is due only to that emitted from the ground,

$$I(\tau_1, +\mu) = I_\nu. \tag{7}$$

The plus and minus signs signify upward and downward directions respectively. The radiative transfer equation is solved using the discrete ordinates method (Chandrasekhar, 1960; Liou, 1973; Stamnes & Swanson, 1981). It can be shown that the solution to Eq. (5) may be written

$$I(\tau, \mu_i) = \sum_j L_j W_j(\mu_i) \exp(-k_j \tau) + B(T) \tag{8}$$

with $-n \le i, j \le n$, where $2n$ is the number of discrete radiation streams. The eigenvalues, k_j and eigenvectors W_j are determined by using an algebraic eigenvalue equation solver as suggested by

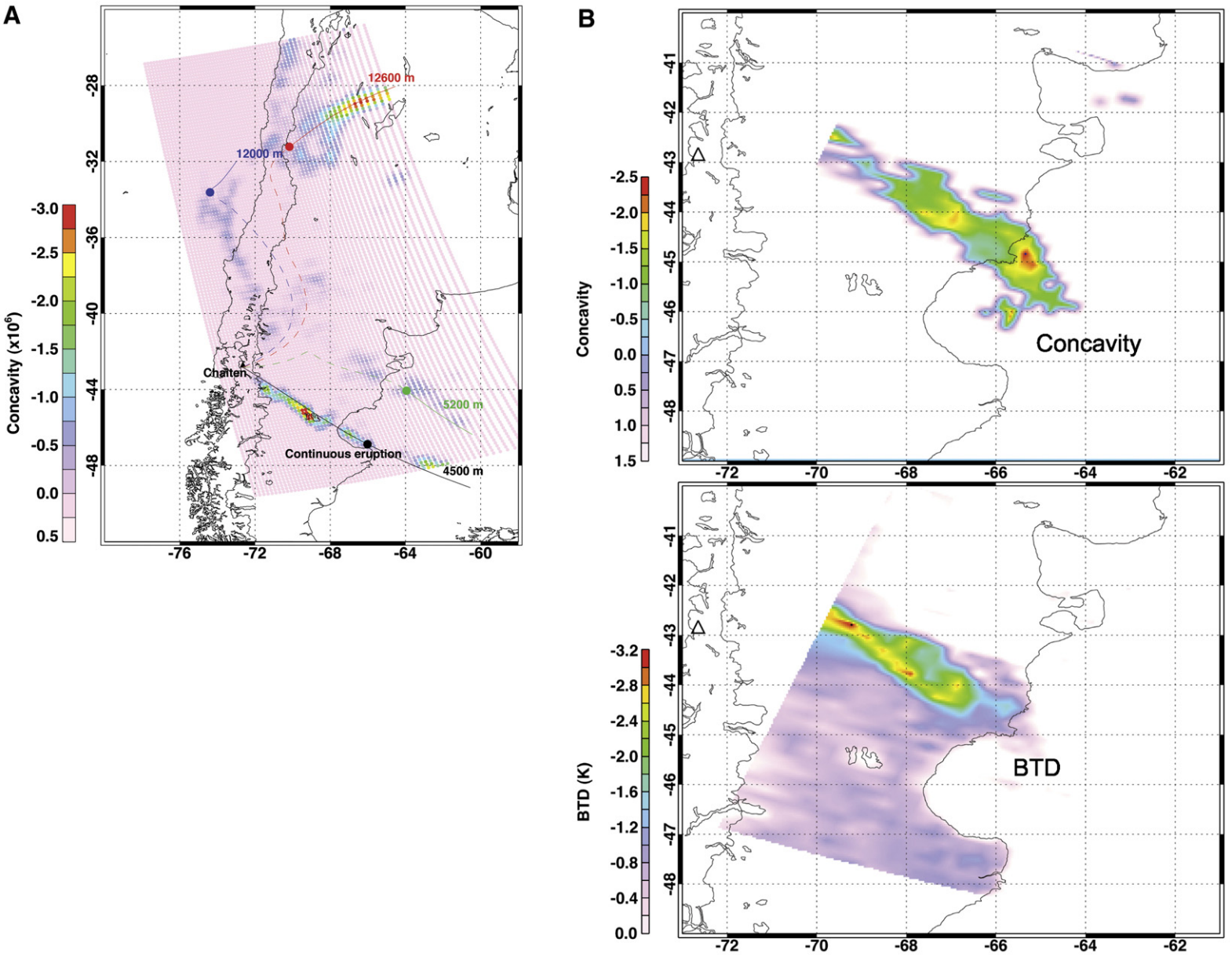

Fig. 3. (A) Concavity map for two consecutive AIRS granules obtained on 3 May 2008 between 18:41–18:53UT (AIRS granule 187 and 188). Negative concavity is indicative of ash—a stronger ash signal leads to a more negative concavity. The Concavity, $\mathcal{C}$, has been multiplied by a factor of 10^6 for ease of plotting. HSYPLIT trajectories for four possible plume paths are also shown on the plot, at 4500, 5200, 12,100 and 12,600 m. The dots indicate the times along the transect when the image data were acquired. (B) Top: Concavity for an AIRS granule obtained on 5-May 2008 at 04:53 UT. Bottom: Reverse absorption temperature difference for a MODIS/Aqua image obtained contemperaneously with the AIRS measurements.

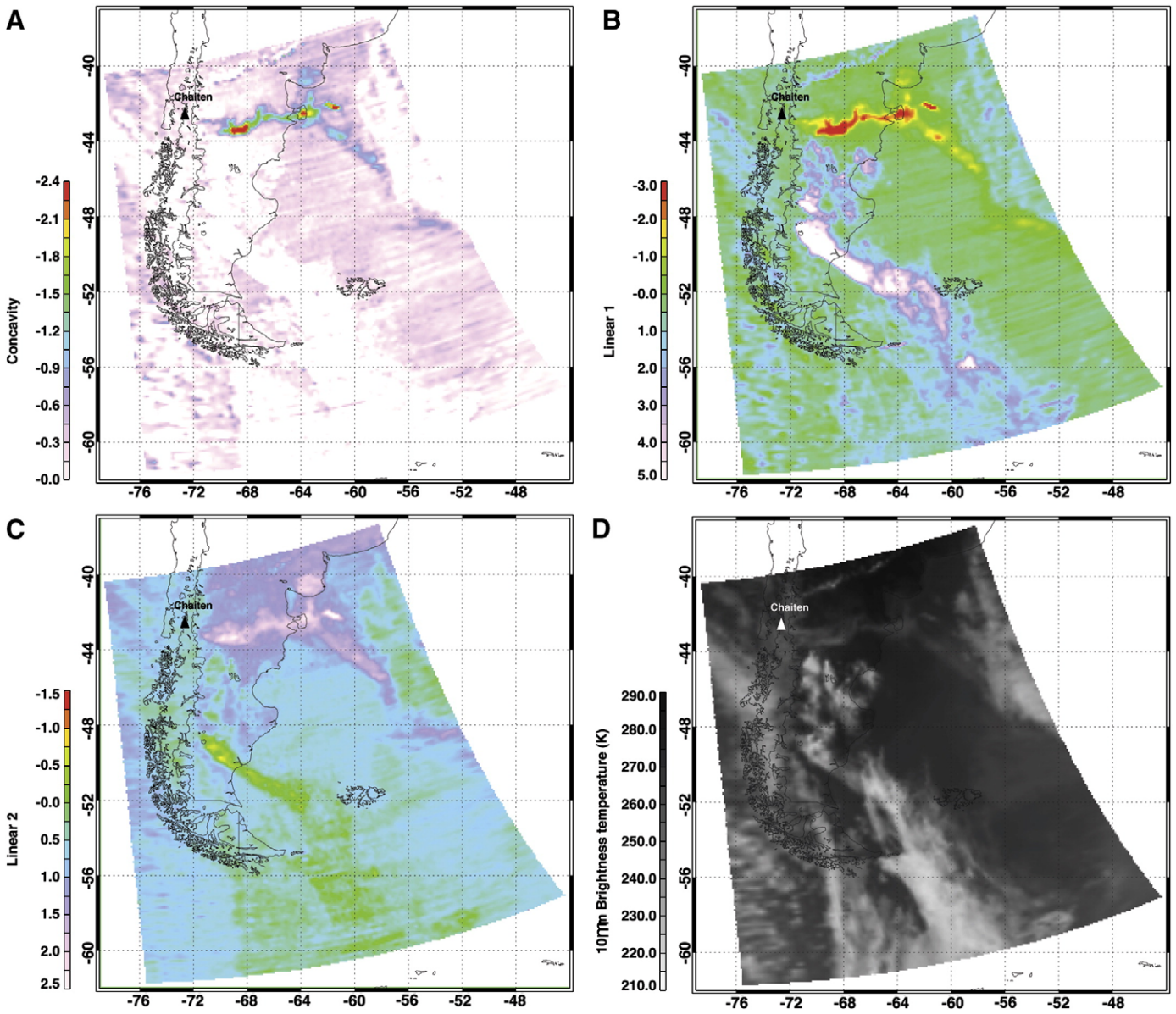

Fig. 4. (A) The concavity ($\times 10^6$) for an eruption cloud of Chaitén on 3 May 2008. (B) An image of the slope ($\times 10^4$) for the linear fit of the spectra between 910 and 980 cm^{-1} for the same data as shown in (A). (C) Same as (B) but for the slope ($\times 10^4$) of the linear fit of the spectra between 1070 and 1130 cm^{-1}. (D) Image of the 10 μm brightness temperature (in Kelvin) for the same eruption.

Stamnes and Swanson (1981). The constants of integration, L_j are determined from the boundary conditions. The lower boundary condition requires an estimate of the surface temperature and surface spectral emissivity, which in general are not available. The surface temperature can be obtained from other contemporaneous satellite measurements (e.g. MODIS), but the spectral emissivity must be specified. For this work we attempt to simulate the radiative transfer for the ash cloud over the sea–sea surface temperature measurements were obtained from the GODAE High Resolution Sea Surface Temperature Pilot Project (GHRSST—http://www.ghrsst-pp.org/GHRSST-PP-data-servers.html) and the sea surface emissivity was assumed to be spectrally flat with a value of 0.985 (Wu & Smith, 1997). Estimation of the surface emission over bare and sandy surfaces may confound the retrieval because it is known that these surfaces have significant spectral emissivity variation in the 800–1200 cm^{-1} range. To properly simulate the brightness temperature spectra incident at the lower boundary of the ash cloud would require greater attention to estimating the surface temperature over the land and a model of the spectral emissivity dependence of the land and ocean.

The second stage of the radiative transfer consists of calculating the scattered radiation leaving the top of the layer, as a function of zenith angle, particle size and optical depth, again at each AIRS wavenumber. The calculation requires a model for the effects of scattering by the particles. A Mie code has been used initially, as scattering by spheres is well understood and we have no information on the true shapes of the scatterers in the ash cloud, although it is unlikely they are spherical. The size distribution used was a modified gamma distribution, but calculations were also done using a log-normal distribution. There are very few measurements of particle size distributions of volcanic clouds in the first few days of residence. Chuan et al. (1981) and Farlow et al. (1981) reported measurements for the Mt St Helens volcanic cloud and found monomodal and multimodal size distributions with silicate ash particle radii typically < 5 μm. These could be modelled using the log-normal distribution. Turco et al. (1983) have developed a sophisticated microphysical

model of an evolving volcanic cloud. They use a bimodal size distribution to represent silicate ash particles with a dominant mode at 3 μm radius containing 97% of the mass, and a mode with radius 0.5 μm containing the remaining mass. Wen and Rose (1994) and Prata and Grant (2001) have shown that the retrievals of particle size and mass are sensitive to the assumed size distribution and complex index of refraction. In this paper we are not attempting to perform quantitative retrievals, but rather explore the principal effects of the particle sizes and composition on the shape of the infrared spectra.

The Mie code requires the complex index of refraction of the particles as a function of wavenumber, ideally provided at the AIRS wavenumbers. Such data are difficult to obtain and we have used the refractive indices of andesite and obsidian (rhyolite) from Pollack et al. (1973), interpolated to the AIRS wavenumbers from their original tabulations. Andesite and rhyolite differ in their composition by, principally, the amount of SiO_2 they contain. The imaginary part of the index of refraction (n_i) affects the ability of the particle to absorb radiation. Both andesite and rhyolite have broad peaks in n_i between 800 and 1130 cm^{-1}; the peak for rhyolite is shifted towards longer wavenumbers and is narrower. Pure quartz refractive indices (Steyer et al., 1974) were also used in the simulations. We expect these compositional effects to be manifested in the AIRS spectra.

Particle size was varied from 0.25 μm radius up to 32 μm in steps of 0.25 μm and optical depth from 0.02 to 3 in steps of 0.02, at a reference wavenumber of 1000 cm^{-1}. At the conclusion of the simulations, 128 (particle size bins) × 150 (optical depth bins) × 3 (compositional bins) of brightness temperature spectra were available for comparison with the AIRS measurements. Fig. 5 illustrates the results for an AIRS pixel affected by the Chaitén ash plume. The black line shows the AIRS brightness temperatures and the coloured lines show radiative transfer simulations for three different particle sizes and two compositions.

For ash containing greater amounts of SiO_2, n_i peaks at higher wavenumbers within this interval, shifting the peak in the concavity towards higher wavenumbers. As particle size increases, the degree of concavity decreases and it seems feasible to retrieve particle size by minimizing the differences between model calculations and AIRS observations. It is noticeable that the degree of agreement is quite sensitive to particle size: better agreement results from a linear combination of two particle sizes (not shown). A further constraint on the fit can be applied by looking at the region between 1070 and 1130 cm^{-1}. The radiative transfer modelling suggests that the majority of particle sizes are not smaller than 1 μm (radius) and not larger than 2 μm in this plume. The refractive index data for rhyolite was found to give much better fits than either andesite or quartz, and as the ash in the Chaitén eruption cloud was found to be rhyolitic (Carn et al., 2009), this is an encouraging result. The rhyolite ('obsidian') simulations fail to accurately reproduce the peak in the transmission near 840–850 cm^{-1} and this may be due to the representativeness of the refractive index data used, which has a peak in n_i between 1000 and 1100 cm^{-1}. A laboratory measured transmission spectrum of a sample of rhyolite (http://pyrite.geo.stonybrook.edu/spectral-database/spectra/index.htm) shows a peak in the transmission curve between 850 and 860 cm^{-1}; these and other data suggest that ash, dust and mineral particles exhibit a wide range of optical properties (Volz, 1973; Sokolik et al., 2001). The shape of the spectra is also strongly influenced by the infrared optical depth of the ash cloud. As the opacity increases the spectra tend to flatten out and the cloud top behaves like a grey body of high uniform spectral emissivity. On the other hand, at low opacity the spectral shape becomes sensitive to the optical depth. The Appendix provides a simple model to illustrate the effect of opacity on the concavity index.

Although we have not done detailed calculations for desert dust, because the composition of desert dust is different to volcanic ash, the concavity will be different (see Fig. 2). DeSouza-Machado et al. (2006) have examined AIRS spectra to study the effect of desert dust on the opacity at 900 cm^{-1}, and Sokolik (2002) used a line-by-line model with multiple scattering to compute the infrared spectra of mineral dust and found that the slope of the spectra was negative over the 820–920 cm^{-1} region. Our analyses of AIRS data suggest that the spectral curves of mineral dust (desert dust) are quite linear ($C = 0$ or perhaps slightly convex) and fit the simulations using the refractive

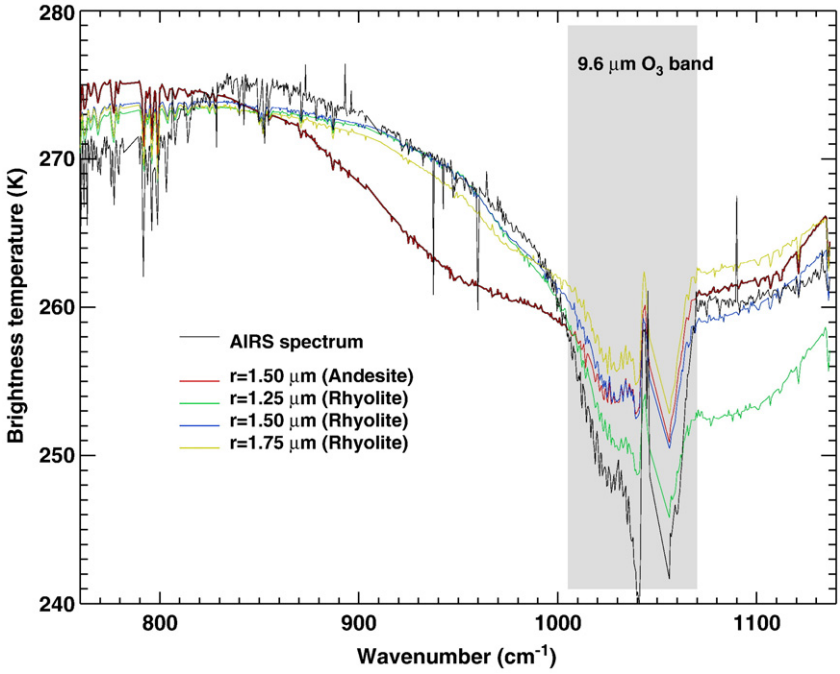

Fig. 5. Measured and modelled AIRS brightness temperature spectra for an eruption of Chaitén volcano on 3 May, 2008. *Black line:* AIRS measurements, *Red line:* particle radius, $r = 1.5$ μm for Andesite; *Green line:* $r = 1.25$ μm for rhyolite (obsidian); *Blue line:* $r = 1.5$ μm for rhyolite; *Yellow line:* $r = 1.75$ μm for rhyolite.

indices of quartz best, also in agreement with DeSouza-Machado et al. (2006).

7. Conclusions

By investigating the shape of the spectra in AIRS measurements for different types of clouds and aerosols we have developed a new algorithm for detecting and discriminating ash clouds from other types of clouds. The principal determinant of whether an AIRS pixel is contaminated with ash appears to be related to the concavity of the spectra within the 800–1000 cm^{-1} region. The concavity is in turn related to the imaginary part of the complex index of refraction of the substance (ash, water, desert dust etc.), the particle size and the infrared opacity. This suggests that high-spectral infrared data may be used to discriminate a variety of airborne mineral substances.

In the case of optically thick clouds, the concavity decreases to zero and the spectra are flat. By contrast, ice and water clouds that are not optically thick have spectral signatures that have a significantly different shape to ash clouds. A potential advantage of using the concavity as a discriminator for volcanic ash is its sensitivity to optically thin clouds. Generally, ash clouds reside in the atmosphere for short periods of time (a few hours to a few days), but it has also been found that ash can be transported over large distances and cause problems for aviation, even at low concentrations, several days after the initial eruption (Tupper et al., 2006). Ash detections using the concavity ($\mathcal{C}$) algorithm for the Chaitén eruption starting on 3 May and ending on 7 May show that this method identifies ash 96 h after the initial eruption and more than 5000 km from the source. Fig. 6 shows C (scaled by a factor 10^6) as coloured points for 19 AIRS granules between 2 and 7 May, 2008 over a region where the Chaitén ash was transported. Although there are no corroborating data to verify ash detection, HYSPLIT trajectories (also shown in Fig. 6 for three different starting altitudes) are consistent with the positions of the $\mathcal{C}$ ash detections. CALIPSO data were examined to look for volcanic aerosols, and two possible detections (shown as inset images in Fig. 6) are suggested on 5 May at around 15:15UT and on 7 May at around 04:50UT. Carn et al.(2009) identified the latter case as an ash cloud. The CALIPSO level 2 browse vertical feature mask product (http://www-calipso.larc.nasa.gov/products/lidar/browse_images/production/) identifies the feature on 5 May as "stratospheric". However, it is difficult to unambiguously identify the Chaitén volcanic aerosol in the Caliop data; this may be due to the lack of significant SO_2 emissions, which in turn suggests that volcanic sulphate aerosol concentrations would have been low. Because methods for unambiguously identifying volcanic ash in the backscatter returns from the Caliop lidar are currently not well developed, these observations must be treated as tentative.

The region between 1070 and 1130 cm^{-1} also appears to be quite sensitive to particle size and can be used together with $\mathcal{C}$ to retrieve particle sizes. Although we have not studied the effects of pixels

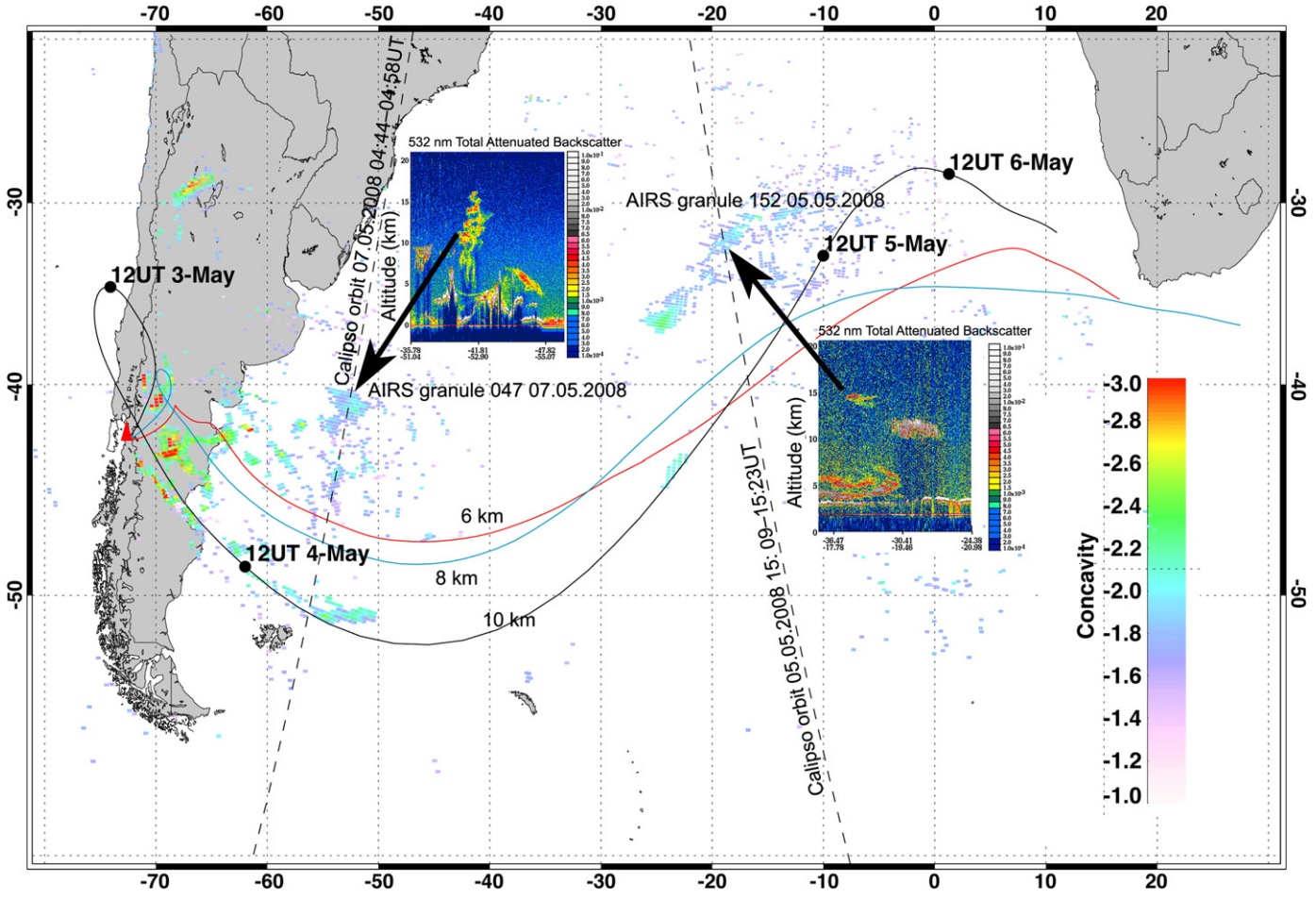

Fig. 6. AIRS pixels identified as volcanic ash using the concavity algorithm for the Chaitén volcanic eruption of 2 May, 2008. AIRS granules covering the geographic region shown and within the time interval 02.05.2008 18:05UT to 06.05.2008 17:35UT were analyzed to calculate $\mathcal{C}$, multiplied by a factor 10^6 and scaled from −3 (red coloured points) to −1 (lilac coloured points). The solid lines are HYSPLIT trajectories for air starting at 6, 8 and 10 km asl from Chaitén at 12:00UT, 2 May 2008, and ending 120 h later. The dashed lines show two CALIPSO orbits; one on 5 May starting at 15:09UT and the other on 7 May starting at 04:44UT. The inset images show cropped portions of the 532 nm total attenuated backscatter ($km^{-1}\,sr^{-1}$) from the Caliop lidar on board CALIPSO. The AIRS granules corresponding to the two CALIPSO orbits are also indicated.

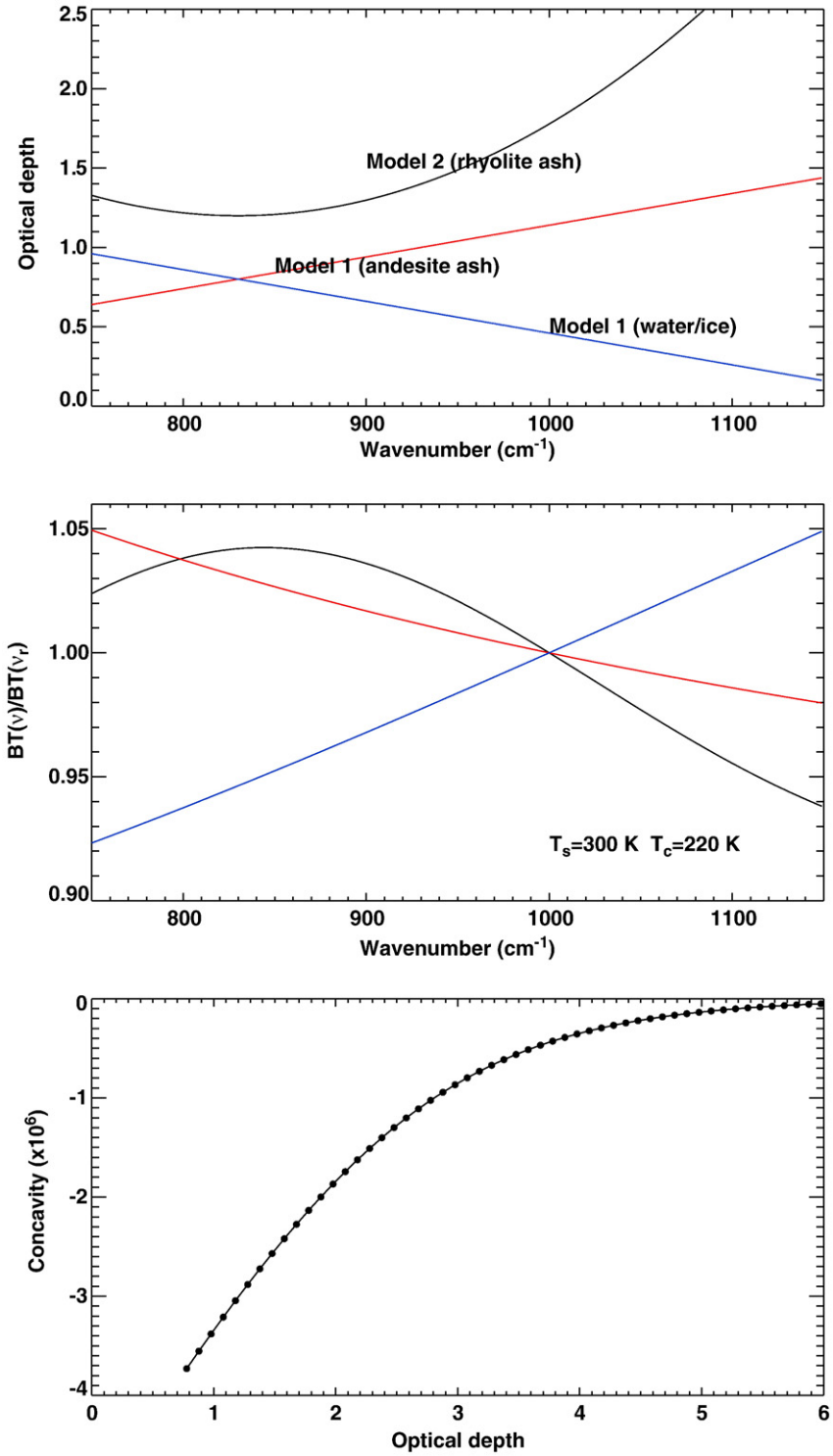

Fig. 7. Top: Three models of the variation of optical depth with wavenumber for water/ice (blue line), andesitic ash (red line) and rhyolitic ash (black line). Middle: Variation of the ratio of brightness temperature (reference wavenumber is 1000 cm^{-1}) for the three models, assuming an emitting surface at 300 K and a cloud top emitting at 220 K. Bottom: Variation of the Concavity with optical depth for the rhyolitic ash optical depth model.

containing mixtures of ash and ice or water clouds, it seems possible that a spectral fitting procedure based on model calculations using refractive indices of ash and ice (or water) may be able to reveal the fractional amounts of the components in the mixtures. In the case of ice coated ash particles this will not be feasible, but comparison of the radiative properties of such particles with AIRS observations is warranted. The high information content of the AIRS spectra should allow much better estimates of the microphysics and radiative properties of ash particles than has been previously possible from multi-spectral imagers such as AVHRR or MODIS. The method is also being extended for use with IASI radiance spectra and this will be reported in a separate paper. By analyzing the spectral signatures in high-spectral resolution infrared data there is potential for diagnosing the constituents of other types of clouds and aerosols, such as smoke

from fires or industrial accidents, windblown desert dust aerosols, volcanic sulphates, and multiphase clouds. We tentatively suggest that the AIRS spectra may be used to retrieve compositional information of airborne volcanic ash, and a more sophisticated approach to the particle size and composition retrieval is under development.

Acknowledgments

L. Clarisse is a Scientific Research Worker (Collaborateur Scientifique) with F. R. S.-FNRS. The research in Belgium was funded by the F. R. S.-FNRS (M. I. S. no. F.4511.08), the Belgian State Federal Office for Scientific, Technical and Cultural Affairs and the European Space Agency (ESA-Prodex arrangements C90-219). Financial support by the "Actions de Recherche Concertées" (Communauté Française de Belgique) is also acknowledged. The authors gratefully acknowledge the NOAA Air Resources Laboratory (ARL) for the provision of the HYSPLIT transport and dispersion model and/or READY website (http://www.arl.noaa.gov/ready.html) used in this publication. This paper is a contribution to the European Space Agency's Support to Aviation for Volcanic Ash Avoidance (SAVAA) project.

Appendix A

The relationship between the infrared optical depth (τ) and $\mathcal{C}$ is explored here using a simple parametric model of the radiative transfer with no scattering. The ash cloud layer is assumed to be a plane-parallel isothermal layer with temperature T_c and radiation from below the cloud is characterised with a uniform temperature T_s. The cloud microphysics (ash, water or ice) is represented by an optical depth function τ_ν and for the purpose of illustration only, two simple models are specified:Model 1 (linear dependence):

$$\tau_\nu = \alpha + \beta\nu. \tag{9}$$

Model 2 (quadratic dependence):

$$\tau_\nu = \alpha' + \beta'(\nu - \nu_0)^2, \tag{10}$$

where α, β, α' and β' are parameters to be specified and ν_0 represents the wavenumber of peak optical depth for the quadratic model. Model 1 with $\beta > 0$ is a simple representation of the variation of optical depth with wavenumber in the 800–12,000 cm^{-1} interval for water clouds (e.g. Chyleyk & Damiano, 1992; Chylek & Ramaswamy, 1982) and ice clouds (e.g. Smith et al., 1993; Yang et al., 2005 and Fu et al., 1998).In the zero-scattering approximation (Paltridge & Platt, 1976), the infrared transmission (t) is related to the optical depth of the cloud through,

$$t_\nu = \exp(-k_\nu z), \tag{11}$$

$$\tau_\nu = k_\nu z, \tag{12}$$

where k_ν is the absorption coefficient and z is the cloud's geometrical thickness. For this simple model, the spectral radiance emerging at the top of the cloud may be written,

$$R_\nu = (1-t_\nu)B_\nu(T_s) + t_\nu B_\nu[T_c], \tag{13}$$

where B_ν is the Planck function. In reality the spectral radiance incident at the lower boundary of the cloud is not uniform, because of absorption and emission of radiation by gases between the earth's surface and the ash cloud and because the radiation emitted by the surface is not uniform—since both the surface temperature and the spectral emissivity of the surface may be varying. There is also reflected radiation at the top of the cloud from atmospheric gases above the cloud, and emission from the atmosphere above the cloud. However, for sufficiently high clouds, with cloud tops near the tropopause, it can be shown that this contribution is small in comparison to the radiation emitted by the cloud. These other effects that are not included in this model do not alter the principal physics of the problem and will be explored in greater detail in a second paper. The Concavity is calculated from fitting the variable $F_\nu = B^{-1}[R_\nu]/B^{-1}[R_{\nu_r}]$, as a function of ν over the 780–880 cm^{-1} interval, where ν_r is the reference wavenumber ($\nu_r = 1000\ cm^{-1}$), and B^{-1} is the inverse of the Planck function. The variation of τ_ν and F_ν with ν are shown in Fig. 7 for the two optical depth models with $\nu_0 = 850\ cm^{-1}$. Model 1 is supposed to be representative of water vapour or water/ice cloud absorption ($\beta > 0$) or andesitic ash cloud absorption ($\beta < 0$). In these cases $\frac{\partial^2 F}{\partial \nu^2} = 0$ and the Concavity will also be 0. Model 2 represents rhyolitic ash with $\beta' > 0$ and as can be seen F_ν has a peak at ν_0 corresponding to the position of the peak in optical depth. The variation of $\mathcal{C}$ with optical depth for Model 2 is shown in the bottom panel of Fig. 7. As the optical depth increases $\mathcal{C}$ increases (becomes more positive), eventually reaching 0. At this point, despite the strong variation of τ_ν with ν, the cloud is so thick that it appears grey (or black) and the radiance spectra are flat. Note also that the $\mathcal{C}$ is most negative at low optical depth demonstrating the sensitivity to low opacity ash clouds. Despite the simplicity of the models used, the results agree with the AIRS spectral measurements for Chaitén ash (rhyolite, Model 2), for Etna ash (Model 1) and for water/ice clouds (Model 1).

References

Berk, A., Anderson, G. P., Bernstein, L. S., Acharya, P. K., Dothe, H., Matthew, M. W., et al. (1999). MODTRAN4 radiative transfer modeling for atmospheric correction. *SPIE proceeding, optical spectroscopic techniques and instrumentation for atmospheric and space research III* (pp. 3756).

Carn, S. A., Pallister, J. S., Lara, L., Ewert, J. W., Watt, S., Prata, A. J., Thomas, R., & Villarosa, G. (2009). The re-awakening of Chaitén volcano. *EOS.*, *90*(24), 2005−2006.

Casadevall, T. J., Delos Reyes, P. J., & Schneider, D. J. (1996). The 1991 Pinatubo eruptions and their effects on aircraft operations. In R. S. Punongbayan (Ed.), *Fire and mud: Eruptions and lahars of Mount Pinatubo, Philippines, Quezon City: Philippines Institute of Volcanology and Seismology*. (pp. 625−636) Seattle: University of Washington Press.

Chahine, M. T., et al. (2006). AIRS: Improving weather forecasting and providing new data on greenhouse gases. *Bull. Am. Meteorol. Soc.*, *87*(7), 911−926. doi:10.1175/BAMS-87-7-911

Chandrasekhar, S. (1960). *Radiative transfer* New York, U. S. A: Dover Publications Inc.

Chuan, R. L., Woods, D. C., & McCormick, M. P. (1981). Characterization of aerosols from eruptions of Mount St. Helens. *Science*, *211*, 830−832.

Chyleyk, P., & Damiano, P. (1992). Infrared emittance of water clouds. *J. Atmos. Sci.*, *49*(16), 1459−1472.

Chylek, P., & Ramaswamy, V. (1982). Simple approximation for infrared emissivity of water clouds. *J. Atmos. Sci.*, *39*, 171−177.

DeSouza-Machado, S. G., Strow, L. L., Hannon, S. E., & Motteler, H. E. (2006). Infrared dust spectral signatures from AIRS. *Geophys. Res. Lett.*, *33*, L03801. doi:10.1029/2005GL024364

Draxler, R. R., & Rolph, G. D. (2003). HYSPLIT (Hybrid Single-Particle Lagrangian Integrated Trajectory) model access via NOAA ARL READY Website Silver Spring, MD, USA: NOAA Air Resources Laboratory.

Ellrod, G. P., Connell, B. H., & Hillger, D. W. (2003). Improved detection of airborne volcanic ash using multispectral infrared satellite data. *J. Geophys. Res.*, *D12*, 4356. doi:10.1029/2002JD002802

Farlow, H. N., Oberbeck, V. R., Snetsinger, K. G., Ferry, G. V., Polkowski, G., & Hayes, D. M. (1981). Size distributions and mineralogy of ash particles in the stratosphere from eruptions of Mt St Helens. *Science*, *211*, 832−834.

Fu, Q., Yang, P., & Sun, W. B. (1998). An accurate parameterization of the infrared radiative properties of cirrus clouds for climate models. *J. Clim.*, *11*, 2223−2237.

Hillger, D. W., & Clark, J. D. (2002). Principal component image analysis of MODIS for volcanic ash. Part I: Most important bands and implications for future GOES imagers. *J. Appl. Meteorol*, *41*, 985−1001.

Hillger, D. W., & Clark, J. D. (2002). Principal component image analysis of MODIS for volcanic ash. Part II: Simulation of current GOES and GOES-M imagers. *J. Appl. Meteorol.*, *41*, 1003−1010.

Li, J., Huang, H. -L., Liu, C. -Y., Yang, P., Schmit, T. J., Wei, H., Weisz, E., Guan, L., & Menzel, P. (2005). Retrieval of cloud microphysical properties from MODIS and AIRS. *J. Appl. Meteorol.*, *44*, 1526−1543.

Liou, K. -N. (1973). A numerical experiment on Chandrasekhar's discrete-ordinate method for radiative transfer: Applications to cloudy and hazy atmospheres. *J. Atmos. Sci.*, 1303−1326.

Paltridge, G. W., & Platt, C. M. R. (1976). Radiative processes in meteorology and climatology. Elsevier 318 pp.

Pavolonis, M. J., Feltz, W. F., Heidinger, A. K., & Gallina, G. M. (2006). A daytime complement to the reverse absorption technique for improved automated detection of volcanic ash. *J. Atmos. Oceanic Technol.*, *23*, 1422−1444.

Pergola, N., Tramutoli, V., Marchese, F., Scaffidi, I., & Lacav, T. (2004). Improving volcanic ash cloud detection by a robust satellite technique. *Rem. Sens. Environ.*, *90*, 1−22.

Pollack, J. B., Toon, O. B., & Khare, B. K. (1973). Optical properties of some terrestrial rocks and glasses". *Icarus*, *19*, 372−389.

Prata, A. J. (1989). Radiative transfer calculations for volcanic ash clouds. *Geophys. Res. Lett.*, *16*(11), 1293−1296.

Prata, A. J., & Grant, I. F. (2001). Retrieval of microphysical and morphological properties of volcanic ash plumes from satellite data: Application to Mt. Ruapehu, New Zealand. *Q. J. R. Meteorol. Soc.*, *127*, 2153−2179.

Prata, A. J., Bluth, G. J. J., Rose, W. I., Schneider, D. J., & Tupper, A. (2001). Comments on "Failures in detecting volcanic ash from a satellite-based technique". *Remote Sens. Environ.*, *78*, 341−346.

Simpson, J. J., Hufford, G., Pieri, D., & Berg, J. (2000). Failures in detecting volcanic ash from a satellite-based technique. *Remote Sens. Environ.*, *72*, 191−217.

Simpson, J. J., Hufford, G., Pieri, D., & Berg, J. S. (2001). Response to comments on "Failures in detecting volcanic ash from a satellite-based technique". *Remote Sens. Environ.*, *72*, 347−357.

Smith, W. L., Ma, X. L., Ackerman, S. A., Revercomb, H. E., & Knuteson, R. O. (1993). Remote sensing cloud properties from high spectral resolution infrared observations. *J. Atmos. Sci.*, *50*(12), 1708−1720.

Sokolik, I. N., Winker, D., Bergametti, G., Gillette, D., Carmichael, G., Kaufman, Y., Gomes, L., Schuetz, L., & Penner, J. (2001). Introduction to special section on mineral dust: Outstanding problems in quantifying the radiative impact of mineral dust. *Geophys. Res.*, *106*, 18,015−18,027.

Sokolik, I. N. (2002). The spectral radiative signature of wind-blown mineral dust: Implications for remote sensing in the thermal IR region. *Geophys. Res. Lett.*, *29*(24), 2154. doi:10.1029/2002GL015910

Stamnes, K., & Swanson, R. A. (1981). A new look at the discrete ordinates method for radiative transfer calculations in anisotropically scattering atmospheres. *J. Atmos. Sci.*, *38*, 387−399.

Steyer, T. R., Day, K. L., & Huffmann, D. R. (1974). Infrared absorption by small amorphous quartz spheres. *Appl. Optics*, *13*(7), 1586−1590.

Tupper, A., Carn, S., Davey, J., Kamada, Y., Potts, R., Prata, A., & Tokuno, M. (2004). An evaluation of volcanic cloud detection techniques during recent significant eruptions in the western Ring of Fire. *Rem. Sensing Environ.*, *91*, 27−46.

Tupper, A., Davey, J., Stewart, P., Stunder, S., Servranckx, R., & Prata, A. (2006). Aircraft encounters with volcanic clouds over Micronesia, Oceania, 2002–2003. *Aust. Met. Mag.*, *55*, 289−299.

Turco, R. P., Toon, O. B., Whitten, R. C., Hamill, P., & Keesee, R. G. (1983). The 1980 eruptions of Mount St. Helens' physical and chemical processes in the stratospheric clouds. *J. Geophys. Res.*, *88*(C9), 5299−5319.

Volz, F. E. (1973). Infrared optical constants of ammonium sulfate, Sahara dust, volcanic pumice, and flyash. *Appl. Opt.*, *12*(3), 564−568.

Wen, S., & Rose, W. I. (1994). Retrieval of sizes and total masses of particles in volcanic clouds using AVHRR bands 4 and 5. *J. Geophys. Res.*, *99*(D3), 5421−5431.

Wu, X., & Smith, W. L. (1997). Emissivity of rough sea surface for 8–13 μm: Modeling and verification. *Appl. Opt.*, *36*, 2609−2619.

Yang, P., Wei, H., Huang, H. -L., Baum, B. A., Hu, Y. X., Kattawar, G. W., Mishhchenko, M. I., & Fu, Q. (2005). Scattering and absorption property database for nonspherical ice particles in the near-through far-infrared spectral region. *Appl. Opt.*, *44*(26), 5512−5523.

Yu, T., Rose, W. I., & Prata, A. J. (2002). Atmospheric correction for satellite-based volcanic ash mapping and retrievals using split window IR data from GOES and AVHRR. *J. Geophys. Res.*, *107*(D16), 43110-4311. doi:10.1029/2001JD000706